View metadata, citation and similar papers at core.ac.uk

brought to you by CORE

provided by University of Strathclyde Institutional Repository

Strathprints Institutional Repository

Wang, Enhao and Xiao, Qing and Srinil, Narakorn and Zanganeh, Hossein (2013) *Vortex-induced vibration of circular cylinder with two degrees of freedom : CFD vs. reduced-order models.* In: 32nd Int Conf on Offshore Mechanics and Arctic Engineering (OMAE2013), 2013-06-09 - 2013-06-14, Nantes.

Strathprints is designed to allow users to access the research output of the University of Strathclyde. Copyright © and Moral Rights for the papers on this site are retained by the individual authors and/or other copyright owners. You may not engage in further distribution of the material for any profitmaking activities or any commercial gain. You may freely distribute both the url (http://strathprints.strath.ac.uk/) and the content of this paper for research or study, educational, or not-for-profit purposes without prior permission or charge.

Any correspondence concerning this service should be sent to Strathprints administrator: mailto:strathprints@strath.ac.uk

http://strathprints.strath.ac.uk/

Proceedings of the ASME 2013 32nd International Conference on Ocean, Offshore and Arctic Engineering
OMAE2013
June 9-14, 2013, Nantes, France

OMAE2013-10456

VORTEX INDUCED VIBRATION OF CIRCULAR CYLINDER WITH TWO DEGREES OF FREEDOM: COMPUTATIONAL FLUID DYNAMICS VS. REDUCED-ORDER MODELS

Enhao Wang, Qing Xiao, Narakorn Srinil, Hossein Zanganeh
Department of Naval Architecture and Marine Engineering, University of Strathclyde,
Glasgow, Scotland, UK

ABSTRACT

Computational fluid dynamics (CFD) studies capturing vortex-induced vibration (VIV) phenomena in a wide range of both the hydrodynamics and the structural parameters are important, because the analysis outcomes can be applied to numerical prediction codes, complement experimental measurement results and suggest a modification of some practical design guidelines. Nevertheless, in spite of many published studies on VIV, CFD studies for two dimensional coupled cross-flow/in-line VIV even with two degrees of freedom (2-DoF), are still quite limited. More CFD studies which can control the equivalence of system fluid-structure parameters in different directions with reduced uncertainty are needed to improve the numerical model empirical coefficients and capability to effectively match numerical predictions and experimental outcomes.

This paper presents a CFD study on the 2-DoF VIV of elastically mounted circular cylinder with a low mass ratio (m^*=2.55). The Reynolds number is fixed to be 150 and the reduced flow velocity parameter is varied by changing the cross-flow natural frequency. To model the problem, two-dimensional Navier-Stokes equations coupled with linear structural equations in the in-line and cross-flow directions are solved. Particular attention is paid to the determination of maximum attainable amplitudes and the associated instantaneous lift and drag forces and hydrodynamic coefficients. These results are compared with the obtained results from alternative numerical prediction outcomes using new reduced-order models with four nonlinearly coupled wake-structure oscillators (Srinil and Zanganeh, 2012). Some qualitative and quantitative aspects are discussed. Overall, the important VIV characteristics are captured including the dual-resonance and figure-of-eight trajectories. Through the flow visualization study, it is found that as the dual-resonance is excited, a P+S wake pattern appears.

1. INTRODUCTION

The phenomenon of vortex-induced vibration (VIV) has been of great practical interest in offshore, ocean and subsea engineering. It is well known that when a bluff body is placed in a fluid flow, the fluid-structure interaction gives rise to VIV. Cylindrical structures are involved in offshore engineering, such as marine cables, mooring lines, pipelines, drilling and production risers and many other hydrodynamic applications. The risk of VIV has become one of the major concerns, which leads to extensive studies on VIV over the past four decades, see, e.g., Sarpkaya (1979), Bearman (1984), Sarpkaya (2004), Williamson and Govardhan (2004), Gabbai and Benaroya (2005) and Bearman (2011).

As the oscillation amplitude in in-line direction is usually smaller than that in the cross-flow direction, transverse VIV of an elastically mounted circular cylinder has been vastly studied, such as Feng (1968), Khalak and Williamson (1996) and Govardhan and Williamson (2004). Feng's results showed that when the vortex shedding frequency approaches the natural frequency of the system, the so-called lock-in phenomenon occurs and this phenomenon usually falls into the reduced velocity range of $5 \leq U_r \leq 7$. Two response branches were found, i.e. the initial and the lower branches. The initial branch is usually associated with 2S wake mode (two single vortices are shed per cycle). In contrast, two pairs of vortices are formed in each vibration cycle (2P mode) in the lower branch. For a cylinder with low mass and damping (quantified by the parameter $m^*\zeta$), a third branch, i.e. the upper branch is discovered by Williamson's group. The 2P mode is also observed in the upper branch. When the mass ratio is further reduced to be less than 6, the effect of in-line motion on the fluid-structure interaction becomes obvious. The maximum transverse vibration amplitude can reach as large as 1.5D (Jauvtis and Williamson, 2004) and the corresponding vortex mode also changes into the 2T mode with two triplets of

vortices being formed each cycle. This new response branch is called the super upper branch.

Singh and Mittal (2005) reported the hysteresis effect in their numerical simulation, and for the first time they observed the P+S mode of vortex shedding (one single vortex is shed at the upper side wake, while a vortex pair forms on the lower side).

Dahl et al. (2010) performed an experiment on the vortex-induced vibration of an elastically mounted circular cylinder at subcritical Reynolds number range (Re=15000-60000) and supercritical Re regime (Re=320000-710000). Their results showed a 'dual resonant' response, which can be described as: the motion in cross-flow direction resonates near the vortex shedding frequency f_v, and the in-line motion resonates at 2 f_v. This occurs over a wide frequency range near the vortex shedding frequency and leads to a highly repeatable figure-eight trajectory. In addition, the third-harmonic components of lift force were observed. The effective natural frequency ratio is found always near 2.0 under the dual-resonance conditions regardless of the nominal natural frequency ratio.

Bao et al. (2012) numerically investigated the effect of natural frequency ratios on flow-induced vibrations of an isolated cylinder and tandem cylinders. The occurrence of dual-resonant response was found to exist over a wide range of natural frequency ratios they tested. A third harmonic frequency component appeared in the lift fluctuation and multiple small peaks of amplitude distributed over a narrow U_r ranging from 4.45 to 5.15. The P+S wake mode is observed when a dual resonance is excited.

Srinil and Zanganeh (2012) proposed an advanced model for predicting a 2-DoF VIV of a flexibly mounted circular cylinder in a uniform flow. Different from linear structural oscillator and van der Pol wake oscillator that were used in previous studies, they developed a model based on double Duffing-van der Pol oscillators with the two structural equations containing both cubic and quadratic nonlinear terms. The predicted results of their model showed a good agreement with several experimental results. Several important VIV characteristics, such as 2-dimensional lock-in, hysteresis phenomenon, and figure-eight trajectory were also captured.

In this work, we present the computational results for 1-DoF and 2-DoF VIV with three different natural frequency ratios. The Reynolds number is fixed as 150. Therefore, a 2-D laminar flow is assumed. The simulation results demonstrate the moving trajectories, amplitudes and hydrodynamic forces of VIV responses. The vortex shedding modes are also shown and analyzed.

The outline of the paper is as follows. A brief description of governing equation for 2-D incompressible flow and the motion equation of rigid bodies is given in Section 3. Section 4 describes how the problem is set up. The results and discussion are given in Section 5, followed by the conclusions.

2. NOMENCLATURE

m^*	Mass ratio
U_r	The reduced velocity
ζ	Damping coefficient
f_v	Vortex-shedding frequency
u, v	Velocity components in stream-wise and transverse directions
m_x, m_y	System mass
c_x, c_y	Damping factor
k_x, k_y	Spring stiffness
F_x, F_y	Hydrodynamic forces in stream-wise and transverse directions
f_{nx}, f_{ny}	Natural frequency in x- and y-direction
$f^*=f_{nx}/f_{ny}$	Natural frequency ratio
f_{nx}, f_{ny}	Natural frequency in stream-wise and transverse directions
x/D, y/D	Dimensionless in-line and cross-flow displacement
ω_{nx}, ω_{ny}	Structural angular velocity
A_x/D, A_y/D	Dimensionless in-line and cross-flow amplitude
C_d	drag coefficient
C_l	lift coefficient

3. NUMERICAL METHOD

3.1 Governing equations

The present simulation is based on a Finite Volume Method (FVM) and the fluid flow is governed by two-dimensional, incompressible, Navier-Stokes equations. The continuity equation and momentum equation in Cartesian Coordinates are given as

$$\frac{\partial u}{\partial x}+\frac{\partial v}{\partial y}=0 \tag{1}$$

$$\frac{\partial u}{\partial t}+u\frac{\partial u}{\partial x}+v\frac{\partial u}{\partial y}=-\frac{1}{\rho}\frac{\partial p}{\partial x}+\nu\left(\frac{\partial^2 u}{\partial x^2}+\frac{\partial^2 u}{\partial y^2}\right) \tag{2}$$

$$\frac{\partial v}{\partial t}+u\frac{\partial v}{\partial x}+v\frac{\partial v}{\partial y}=-\frac{1}{\rho}\frac{\partial p}{\partial y}+\nu\left(\frac{\partial^2 v}{\partial x^2}+\frac{\partial^2 v}{\partial y^2}\right) \tag{3}$$

where u and v are velocity components in x- and y-directions, p is the pressure, ρ is fluid density and ν is the kinematic viscosity of the fluid. The Semi-Implicit Method for Pressure-Linkage Equations (SIMPLE) algorithm is used to solve the pressure-velocity coupled equations. Second-order upwind difference scheme is adopted to deal with the convection terms and a first-order implicit scheme is applied to the unsteady terms in the governing equations.

Copyright © 2013 by ASME

The unstructured mesh is used for the present simulation with a thin layer of structured mesh around the cylinder. The computational mesh used in current simulation is shown in Figure 1. The upstream side has a length of 10D in the negative x-direction and the downstream side has length of 20D in positive x-direction. The upper and lower parts each have 10D in length. The boundary conditions of the computational domain are: the left boundary is defined as velocity inlet; the right boundary is defined as pressure outlet; the upper and lower boundaries have a boundary condition of symmetry and the cylinder is with a no-slip wall boundary condition. Before carrying out the numerical simulations, a mesh refinement test was performed giving the most suitable mesh, in terms of accuracy and computational time, with 200 nodes on the cylinder and 24452 cells in total.

3.2 Equations for an elastically mounted circular cylinder

The motion of an elastically mounted circular cylinder, in x- and y-direction, is governed by the following second-order Ordinary Differential Equations (ODE):

$$m_x\ddot{X} + c_x\dot{X} + k_x X = F_x \tag{4}$$

$$m_y\ddot{Y} + c_y\dot{Y} + k_y Y = F_y \tag{5}$$

where a dot denotes differentiation with respect to time, X and Y stand for the in-line and cross-flow displacements, m, c, k, and F are cylinder mass, system damping coefficient, system stiffness, and hydrodynamic force, respectively. The subscripts x and y indicates the properties in in-line and cross-flow directions. It is assumed that $m_x=m_y=m=m^*\rho\pi D^2/4$, and in order to get a maximum oscillation amplitude, the damping coefficients in both directions are set to be zero, i.e. $c_x=c_y=c=0$.

Eq. 4 and Eq. 5 can be rearranged into implicit functions as

$$f(\dot{X}, X) = \frac{F_x}{m_x} - 2\zeta_x\omega_{nx}\dot{X} - \omega_{nx}{}^2 X \tag{6}$$

$$f(\dot{Y}, Y) = \frac{F_y}{m_y} - 2\zeta_y\omega_{ny}\dot{Y} - \omega_{ny}{}^2 Y \tag{7}$$

Here, u and v are velocity in x- and y-direction respectively. $\zeta_x=\zeta_y=\zeta=c/[2\sqrt{(km)}]$. The angular natural frequency of the system $\omega_{nx}=\sqrt{(k_x/m)}=2\pi f_{nx}$ and $\omega_{ny}=\sqrt{(k_y/m)}=2\pi f_{ny}$.

The forces are assumed to be constant within a sufficient small time step. Thus, Eq. 6 and Eq. 7 can be discretized by using 4th-order Runge-Kutta method.

4. DESCRIPTION OF THE PROBLEM

Simulations are conducted for 1-DoF (cross-flow) VIV and 2-DoF (combined in-line and cross-flow) VIV. The cylinder has a diameter of D and the free stream velocity is denoted by U_∞. The Reynolds number is calculated by $\mathrm{Re}=\rho U_\infty D/\mu$ based on D and U_∞. Although the physical nature of laminar is completely different from that of turbulent flow, the responses of VIV in both laminar and turbulent flow have something in common. In the sense of studying basic response features of VIV, laminar modeling is sufficient to capture characteristic phenomena of VIV, such as the three branches of the amplitude responses, figure-of-eight orbital trajectories and dual resonance. Moreover, compared to turbulence modeling, laminar modeling is simpler and less time-consuming so it can be a good starting point for moving on to the modeling of more complex VIV phenomena. Therefore, studies on 2-DoF VIV associated with laminar flow do have some reference value for more complex VIV phenomenon in terms of flow physics. Thus, the simulations are carried out with a fixed Reynolds number of Re=150. For the Reynolds number $40<\mathrm{Re}<200$, the vortex shedding is essentially two-dimensional, i.e. it does not vary in the span-wise direction (Williamson, 1989). The mass ratio is $m^*=4m/(\rho\pi D^2)$. The reduced velocity $U_r=U_\infty/(f_{ny}D)$ is varied by changing the transverse natural frequency f_{ny}. The reduced velocity ranges from $U_r=3.0$ to $U_r=10.0$ and for each reduced velocity, different frequency ratios are considered, i.e. $f_{nx}/f_{ny}=1.0$, 1.5, and 2.0.

5. RESULTS AND DISCUSSION

5.1 1-DoF VIV: Re=150, varying U_r

Transverse-only VIV is considered first as a validation case. Figure 2 shows how the maximum transverse vibration amplitude varies against the reduced velocity at Re=150, $m^*=2.55$ and $\zeta=0$ as well as other available data. As seen from Figure 2, the present simulation is in good agreement with others' results. The lock-in regime of 1-DoF VIV lies in the U_r range of $4.0<U_r<7.0$. The maximum oscillation amplitude appears at $U_r=4.0$.

5.2 2-DoF VIV: Re=150, varying U_r

The discussion on the 2-DoF VIV will start with the orbital trajectories of the circular cylinder, followed by the cylinder response versus the reduced velocity. The hydrodynamic forces and vortex shedding modes of different U_r at different natural frequency ratios will be presented as well.

5.2.1 Orbital trajectories

Figure 3 shows the orbital trajectory of 2-DoF VIV of a circular cylinder. The results of both CFD simulation and reduced-order model prediction are plotted. From the mechanism of vortex shedding, when each vortex is shed, a fluctuating drag is generated, leading to the in-line instantaneous forcing frequency f_x is twice that of the transverse direction f_y (Bearman, 1984; Naudascher, 1987). As a consequence, the typically orbital trajectory of a circular cylinder undergoing a combined in-line and transverse vibration is of a figure-eight type. This phenomenon is also observed in the present CFD simulation. In Figure 3, the

Copyright © 2013 by ASME

moving trajectories of two cases, i.e. f^*=1.0 and 2.0 are presented. A periodic figure-eight trajectory is observed for all simulations at different U_r as shown in Figure 3 except for the case of f^*=1.0 and U_r=4.0, where an unrepeatable trajectory is observed. In addition, the moving direction of the circular cylinder is labeled with '*C*' or '*CC*', which corresponds to a clockwise and counter-clockwise direction, respectively. In the present simulation, the orbital direction of f^*=1.0 is either clockwise or counter-clockwise. However, at a frequency ratio of f^*=2.0, the cylinder moves only in the counter-clockwise direction. Dahl et al. (2007) related the direction of the orbital trajectory to the high force harmonics. They stated that the cylinder moving upstream at the two extreme ends (counter-clockwise motion) has additional vorticity being generated, which results in a multiple vortex formation and high force harmonics. Triantafyllou et al. (2008) found that the counter-clockwise mode leads to larger fluid forces than the clockwise mode. This will be proved in the following section where the hydrodynamic forces will be discussed.

5.2.2 Cylinder response amplitudes

One of the most important non-dimensional parameters that affects the dynamic characteristics of 2-DoF VIV of a circular cylinder is the mass ratio m^*. It is known that when the mass ratio m^*>6.0, the effect of the in-line oscillation on the transverse vibration is small but when it decreases to m^*<6.0, a dramatic change occurs in the fluid-structure interactions (Jauvtis and Williamson, 2004). As the case in this paper has a relatively small mass ratio, it is of great interest to investigate how the in-line freedom will affect the transverse responses. In Figure 4, a comparison is made between the results of CFD simulation and numerical prediction using a reduced-order model in the amplitude response (in form of dimensionless amplitude vs. U_r).

As is shown in Figure 4 (a), for the CFD simulation results with the natural frequency ratio of f^*=1.0 and 1.5, the non-dimensional amplitudes almost have the same trend against the reduced velocity. The maximum transverse amplitude is observed at U_r=4.0 and its value is approximately 0.6. It has a slight increase as compared to the transverse only (1-DoF) case. However, situation becomes more different when f^* is increased to 2.0. There is a delay in the reduced velocity to U_r=6.0 for the peak amplitude to occur and the maximum value of the non-dimensional amplitude also increase to around 0.8.

A similar increase in the response amplitude is observed for the in-line motion when natural frequency ratio increases with the peak value appears at U_r=4.0 and it reaches a value as high as A_x/D=0.25, which is comparable to the experimental results by Dahl et al. (2010).

5.2.3 Hydrodynamic forces

In the dual-resonant state, the in-line displacements have significant effects on the hydrodynamic force coefficients. To present this, the hydrodynamic force coefficients are drawn against the reduced velocity in Figure 5 for both CFD simulation and reduced-order model prediction.

In terms of the CFD simulation results, A dramatic change can be observed in the oscillating drag coefficient at f^*=2.0, which is nearly three times as large as that at f^*=1.0 and f^*=1.5. On the other hand, the oscillating lift component seems not to change that much as the oscillating drag component.

5.2.4 Vortex shedding modes

When the mass ratio m^* drops to less than 6.0, a dramatic change occurs in the fluid-structure interaction. This change not only happens in the response amplitude, but also takes place in the vortex shedding mode. The so-call 2T mode (a triplet of vortices being formed in each half cycle) was found by Jauvtis and Williamson (2004).

The wake structure in the fully developed vorticity field is presented in Figure 6 for f^*=1.0 and 2.0. 2S mode (two single vortices are shed each cycle) is observed for all the reduced velocities displayed at a natural frequency ratio of f^*=1.0. Although the wake modes are the same for different U_r at f^*=1.0, slight differences still exist in the wake structure for different U_r. For example, a two-row vortex structure is observed for U_r=4.0 and 5.0 in comparison with one-row wake structure in the rest of the cases in Figure 6 (a).

An important change in the wake structure is found at f^*=2.0. At U_r=3.0 and 4.0 the wake retains the 2S mode. However, when the reduced velocity is increased to 5.0, the vortex shedding mode changes into P+S mode (a single vortex and a pair of opposite signed vortices formed each cycle). With a further increase of U_r, the wake mode returns to 2S. A similar result is observed by Sigh and Mittal (2005) and Bao et al. (2012).

5.3 Comparisons with numerical prediction results

By ways of examples, numerical prediction results based on the nonlinearly coupled structure-wake (Duffing-van der Pol) oscillators (Srinil and Zanganeh 2012) are also given in Figures 3-5 in terms of orbital motions, response amplitude diagrams and hydrodynamic force coefficients, respectively, in comparison with CFD results. This reduced-order model (ROM) has been simulated via direct numerical integrations. Note also that the in-line displacements due to the VIV-induced mean drag forces have been removed from prediction results plotted in Figure 4.

Overall comparisons in Figures 4-6 show both qualitative and quantitative differences between the two models: these reflect the challenges in matching the 2-D VIV results which depend on the mathematical models, assumptions, terms and several influencing fluid-structure parameters. For instance, the numerical model has been calibrated based on the experimental results in a higher Re range (whereas the CFD results are based on the fixed Re) and with varying stream-wise and transverse natural frequency (f_{nx} and f_{ny}). Another possible reason might be due to the fact that the numerical model takes into account the effect of geometric cubic-type nonlinear coupling of cross-flow/in-line displacements whereas these features have been disregarded from the CFD model.

Copyright © 2013 by ASME

Nevertheless, as shown by the CFD results, the numerical model captures the dual resonance in which both cross-flow and in-line motions are locked-in with their 2:1 tuned oscillating frequencies, regardless of the specified f^* and there is a phase *x-y* difference observed when varying U_r. In addition, the numerical model shows the effect of varying f^* on the maximum attainable amplitudes and the trend of in-line response seems to be in a good qualitative agreement with CFD analysis. The hydrodynamic coefficients between the two models are different and these are attributed to the fact that the numerical model does not rely on the real flow physics or fluid mechanics. Perhaps overall comparisons would be improved when considering a higher Re range in the CFD study.

6. CONCLUSIONS

A numerical simulation of the vortex-induced vibration of an elastically mounted circular cylinder in the in-line (1-DoF) and combined in-line and cross-flow directions (2-DoF) is carried out at Re=150. A finite volume method is used to solve the governing equations of fluid flow in two dimensions with varying reduced velocity from 1.0 to 10.0. A low mass ratio m^*=2.55 and zero structural damping are considered in the simulation. Three different natural frequency ratios are examined, i.e. f^*=1.0, 1.5 and 2.0. The CFD results are compared with the results from the new reduced-order models.

It is found that the phenomenon of dual-resonance occurs at the values of f^* that tested. The orbital trajectory at f^*=1.0 is either clockwise or counter-clockwise. However, at f^*=2.0, only counter-clockwise direction trajectory is observed. With a low mass ratio used in the simulation, the transverse vibration is significantly amplified by the stream-wise motion. The peak response is also delayed to a higher reduced velocity. The vortex shedding mode of f^*=1.0 is always 2S for the reduced velocity examined, however, for f^*=2.0, P+S mode appears associated with the maximum in-line response.

More parametric studies and comparisons between CFD and numerical prediction models for 2-D VIV in a higher Re range are needed to improve the empirical coefficients of the latter model. Other parameters to be accounted for include the mass, damping and natural frequency ratios.

REFERENCES

Ahn, H. T. & Kallinderis, Y. (2006). Strongly coupled flow/structure interactions with a geometrically conservative ALE sheme on general hybrid meshes. *Journal of Computational Physics, 219*, 671-696.

Bao, Y., Huang, C., Zhou, D., Tu, J. H. & Han, Z. L. (2012). Two-degree-of-freedom flow-induced vibrations on isolated and tandem cylinders with varying natural frequency ratios. *Journal of Fluids and Structures, 35*, 50-75.

Bearman, P. W. (1984). Vortex shedding from oscillating bluff body. *Annual Review of Fluid Mechanics, 16*, 195-222.

Bearman, P. W. (2011). Circular cylinder wakes and vortex-induced vibrations. *Journal of Fluids and Structures, 27*, 648-658.

Borazjani, I. & Sotiropoulou, F. (2009). Vortex-induced vibrations of two cylinders in tandem arrangement in the proximity-wake interference region. *Journal of Fluid Mechanics, 621*, 321-364.

Dahl, J. M., Hover F. S. & Triantafyllou, M. S. (2007). Resonant vibrations of bluff bodies caused multivortex shedding and high frequency forces. *Physical Review Letters, 99*(144503), 144503-1-144503-4.

Dahl, J. M., Hover F. S., Triantafyllou, M. S. & Oakley, O. H. (2010). Dual resonance in vortex-induced vibrations at subcritical and supercritical Reynolds numbers. *Journal of Fluid Mechanics, 643*, 395-424.

Feng, C. C. (1968). *The measurement of vortex induced effects in flow past stationary and oscillating circular and d-section cylinders.* (Master's), University of British Columbia.

Gabbai, R. D. & Benaroya, H. (2005). An overview of modelling and experiments of vortex-induced vibrations of circular cylinders. *Journal of Sound and Vibration, 282*, 575-616.

Govardhan, R. & Williamson, C. H. K. (2000). Modes of vortex formation and frequency response of a freely vibrating cylinder. *Journal of Fluid Mechanics, 420*, 130.

Jauvtis, N. & Williamson, C. H. K. (2004). The effect of two degrees of freedom on vortex-induced vibration at low mass and damping. *Journal of Fluid Mechanics, 509*, 23-62.

Khalak, A. & Williamson, C. H. K. (1996). Dynamics of a hydroelastic cylinder with very low mass and damping. *Journal of Fluids and Structures, 509*, 23-62.

Naudascher, E. (1987). Flow-induced streamwise vibrations of structures. *Journal of Fluids and Structures, 1*, 265-298.

Sarpkaya, T. (1979). Vortex-induced oscillations. *Journal of Applied Mechanics, 46*, 241-258.

Sarpkaya, T. (2004). A critical review of the intrinsic nature of vortex-induced vibrations. *Journal of Fluids and Structures, 19*, 389-447.

Singh, S. P. & Mittal, S. (2005). Vortex-induced oscillations at low Re: Hysteresis and vortex-shedding modes. *Journal of Fluids and Structures, 20*, 1085-1104.

Srinil, N. & Zanganeh, H. (2012). Modelling of coupled cross-flow/in-line vortex-induced vibrations using double Duffing and van der Pol oscillators. *Ocean Engineering, 53*, 83-97.

Triantafyllou, G., Kaiktsis, L., & Peppa, S. (2008). *Hydrodynamic forces on a cylinder vibrating transversely and in-line to a steady stream.* The 61st Annual Meeting of the APS Division of Fluid Dynamics, San Antonio, Texas.

Williamson, C. H. K. . (1989). Oblique and parallel modes of vortex shedding in the wake of a circular cylinder at low Reynolds number. *Journal of Fluid Mechanics, 206*, 597-627.

Williamson, C. H. K. & Govardhan, R. (2004). Vortex-induced vibrations. *Annual Review of Fluid Mechanics, 36*, 413-455.

Williamson, C. H. K. & Govardhan, R. (2008). A brief review of recent results in vortex-induced vibrations. *Journal of Wind Engineering and Industrial Aerodynamics, 96*, 713-735.

Copyright © 2013 by ASME

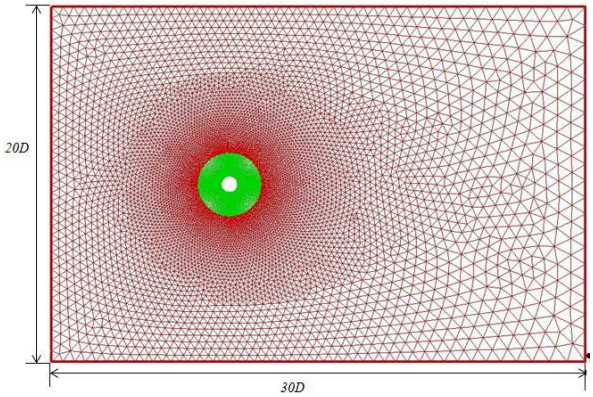

Figure 1. Computational mesh

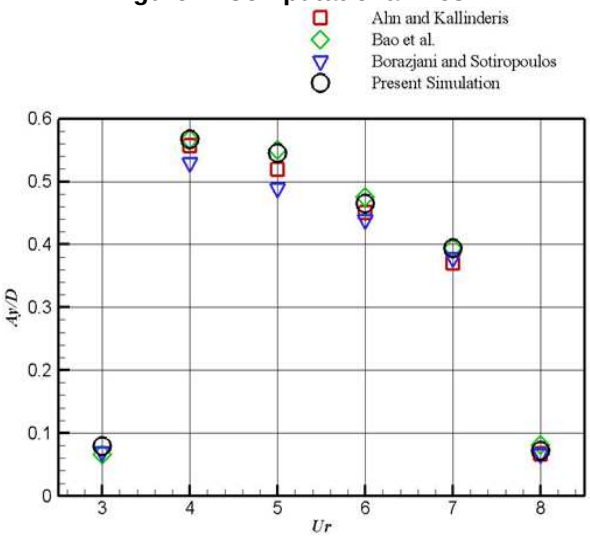

Figure 2. 1-DoF VIV: Re=150, varying U_r

Copyright © 2013 by ASME

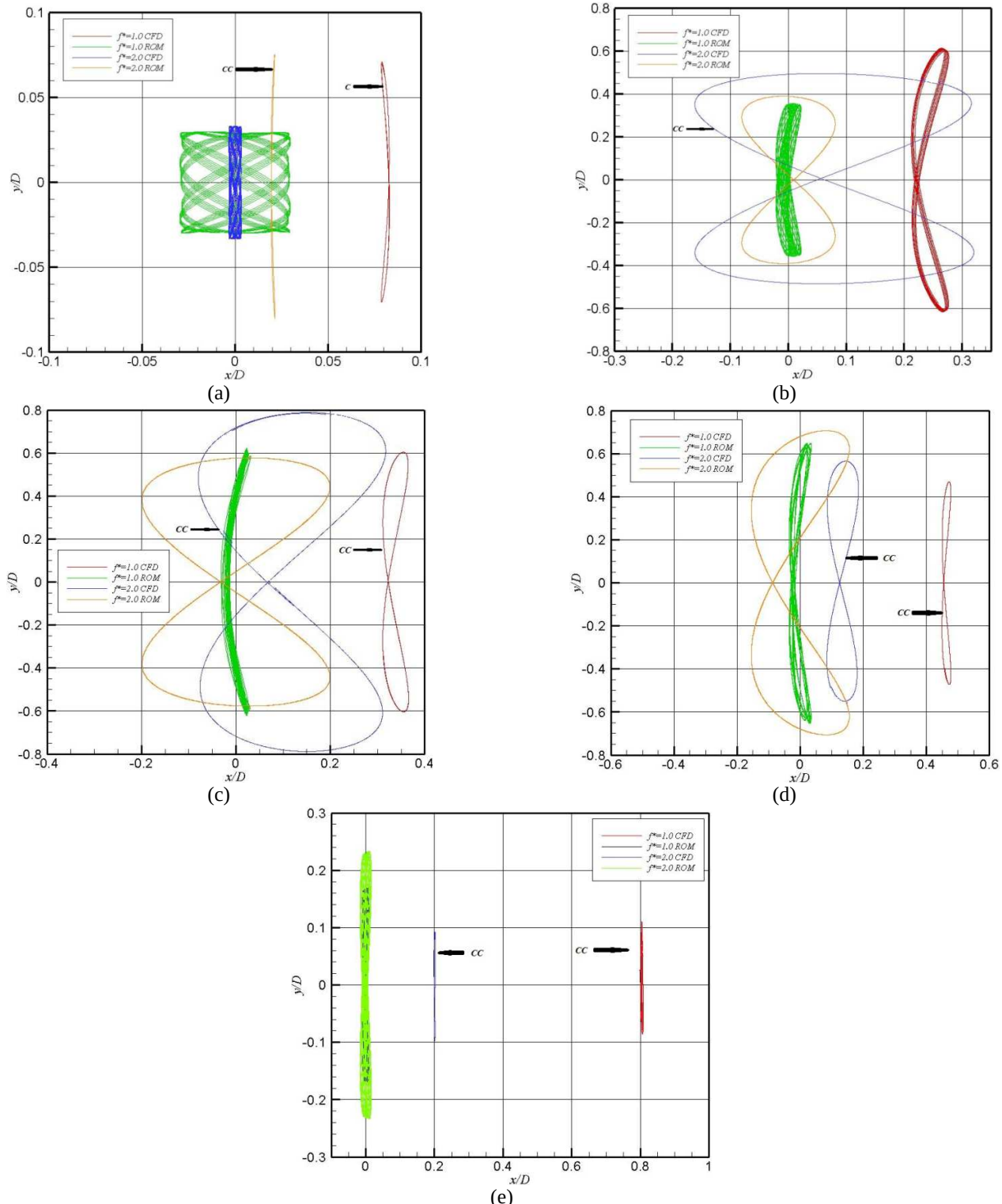

Figure 3. Cylinder orbital trajectories at different f^*: (a) U_r=3.0, (b) U_r=4.0, (c) U_r=5.0, (d) U_r=7.0, and (e) U_r=10.0

Copyright © 2013 by ASME

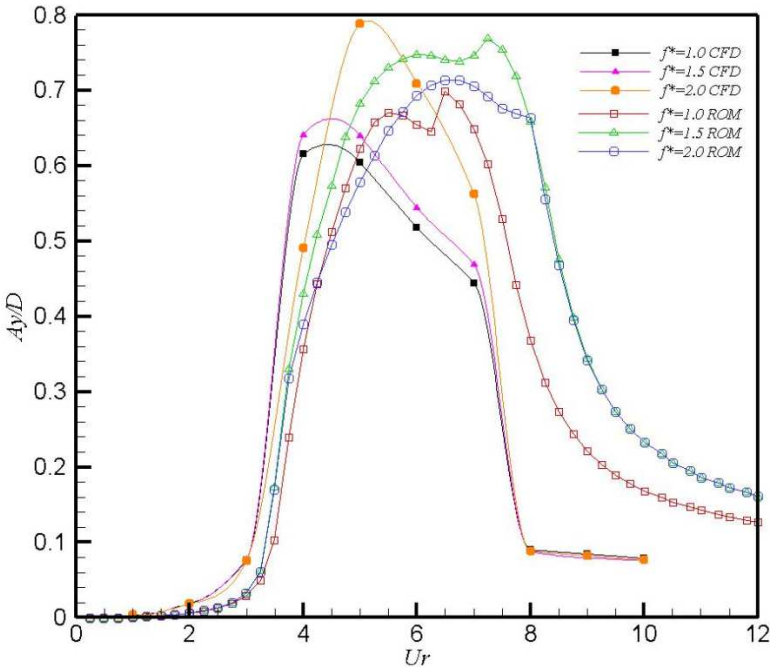

(a)

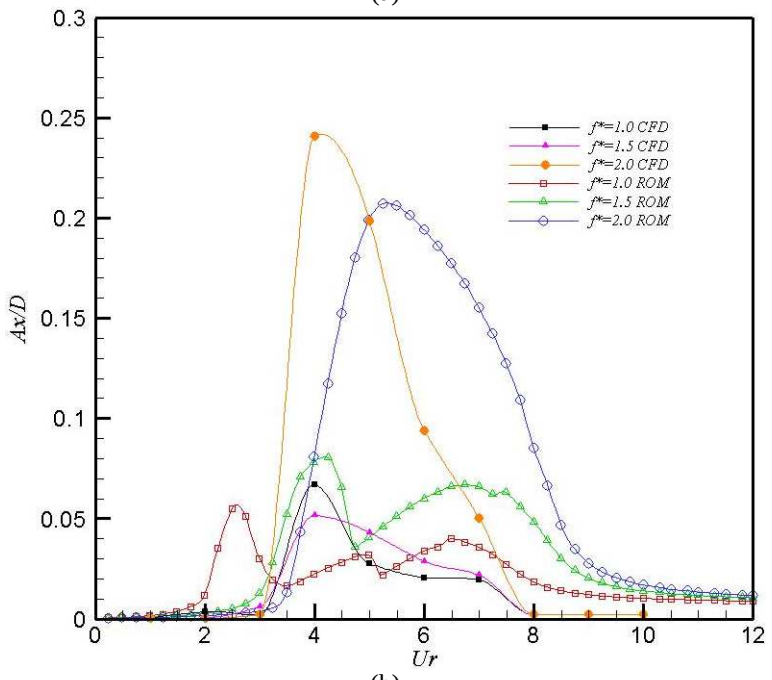

(b)

Figure 4. Dimensionless response amplitude vs. the reduced velocity at different f^*: (a) transverse amplitude, and (b) in-line amplitude

Copyright © 2013 by ASME

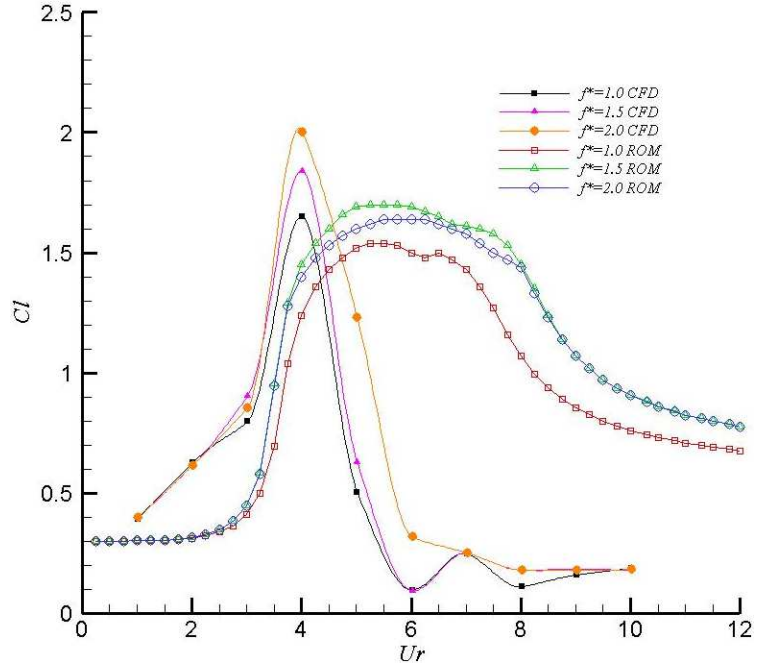

(a)

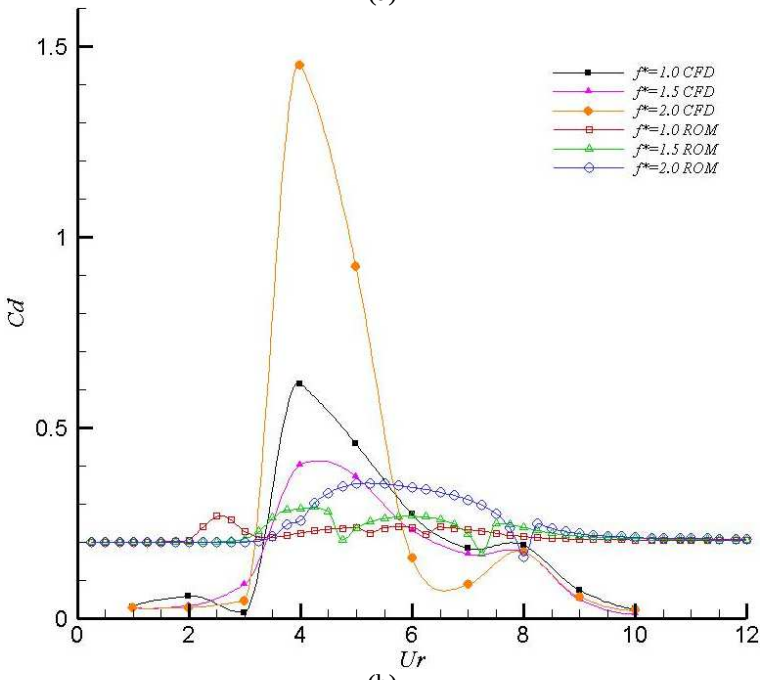

(b)

Figure 5. Hydrodynamic force coefficients vs. the reduced velocity at different natural frequency ratios: (a)maximum value of C_l, and (b) maximum value of oscillating C_d

Copyright © 2013 by ASME

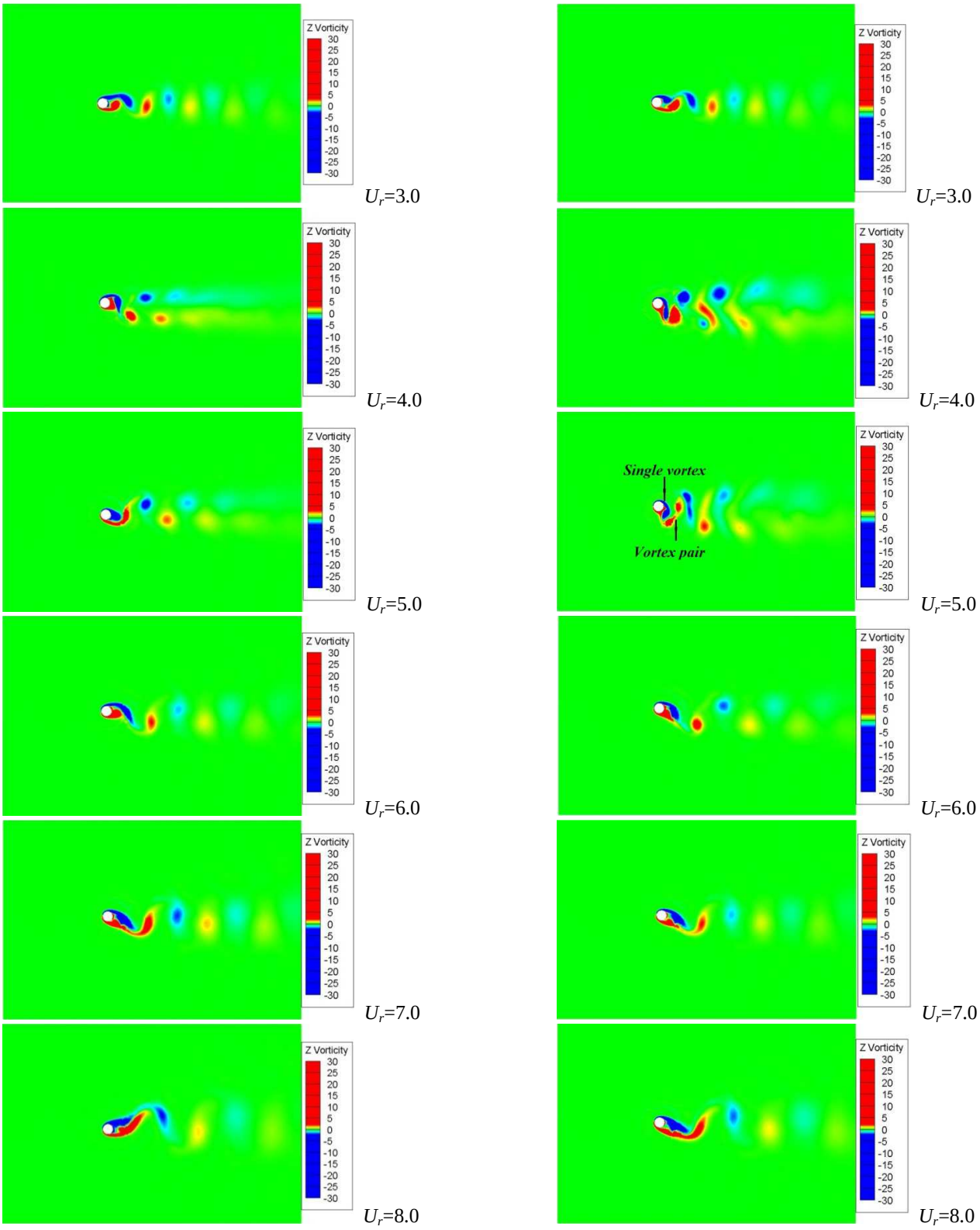

Figure 6. Vortex-shedding modes: (a) f^*=1.0, and (b) f^*=2.0

Copyright © 2013 by ASME